

# Large-scale electron acceleration by parallel electric fields during magnetic reconnection

J. Egedal<sup>1</sup>\*, W. Daughton<sup>2</sup> and A. Le<sup>1</sup>

**Reconnection is the process by which stress in the field of a magnetized plasma is reduced by a topological rearrangement of its magnetic-field lines. The process is often accompanied by an explosive release of magnetic energy and is implicated in a range of astrophysical phenomena<sup>1</sup>. In the Earth's magnetotail, reconnection energizes electrons up to hundreds of keV (ref. 2) and solar-flare events can channel up to 50% of the magnetic energy into the electrons, resulting in superthermal populations in the MeV range<sup>3–5</sup>. Electron energization is also fundamentally important to astrophysical applications<sup>6</sup> yielding a window into the extreme environments. Here we show that during reconnection powerful energization of electrons by magnetic-field-aligned electric field ( $E_{\parallel}$ ) can occur over spatial scales that hugely exceed previous theories and simulations<sup>7</sup>. In our kinetic simulation  $E_{\parallel}$  is supported by non-thermal and strongly anisotropic features in the electron distributions not permitted in standard fluid formulations, but routinely observed by spacecraft in the Earth's magnetosphere. This allows for electron energization in spatial regions that exceed the regular  $d_e$ -scale electron-diffusion region by at least three orders of magnitude.**

Over the past decade, spacecraft have made detailed measurements in the vicinity of reconnection sites in the Earth's magnetotail. In particular, electron distribution functions,  $f$ , have been obtained *in situ*; as an example, in Fig. 1 we consider measurements by the Cluster mission from the much studied event of 1 October 2001 (ref. 8). Previous analyses have established that Cluster 3 passed through a reconnection region as shown in the schematic representation of Fig. 1a (ref. 9), and the distribution in Fig. 1b is typical for the reconnection inflow region, where the electrons are heated in the parallel direction up to 1 keV (from about 100 eV), whereas no energization is observed for the perpendicular direction. In contrast, for the distribution in Fig. 1c observed in the exhaust region, the electrons are heated in both the parallel and the perpendicular directions all the way up to 14 keV. This type of distribution is common in the exhaust close to the reconnection region and is referred to as a flat-top distribution because  $f(\varepsilon)$  is nearly constant (flat) for a large range of energies (here, for  $\varepsilon$  between 1 keV and 14 keV; ref. 10).

Analysis of spacecraft data as well as kinetic simulations shows that the moderate parallel energization of electrons in the inflow region is caused by the acceleration potential  $\Phi_{\parallel} = \int_{\mathbf{x}}^{\infty} E_{\parallel} dl$ , where spatial integration,  $dl$ , from the location,  $\mathbf{x}$ , is carried along magnetic-field lines to the ambient plasma<sup>11</sup>. Thus,  $e\Phi_{\parallel}$  is the energy gained from the parallel electric fields  $E_{\parallel}$  by electrons entering the reconnection region in a straight shot along a magnetic-field line.

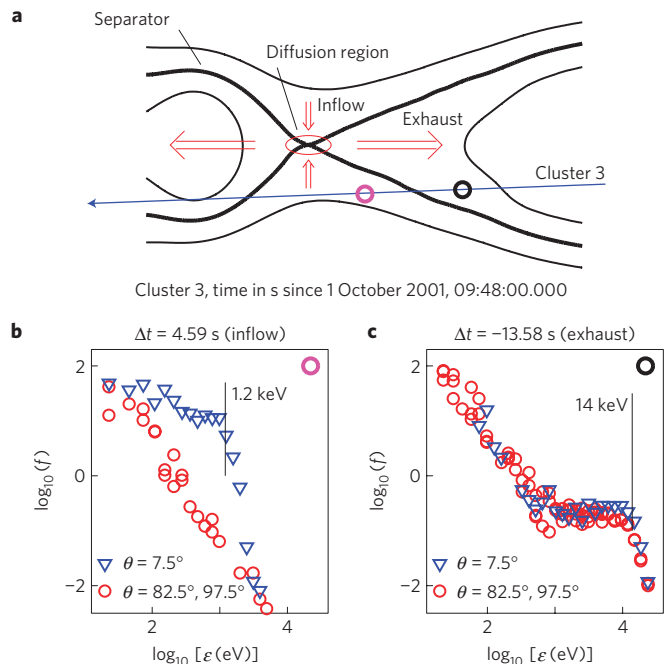


**Figure 1 | Example of strong electron energization recorded by spacecraft in the Earth's magnetotail.** **a**, Schematic of the Cluster mission's encounter with a reconnection region on 1 October 2001. **b, c**, Electron distributions recorded in the inflow region (**a**) and exhaust (**b**) as indicated by the red and black circles, respectively. The data correspond to the parallel direction (along the magnetic field),  $\theta = 7.5^\circ$ , and near-perpendicular directions  $\theta = 82.5^\circ$  and  $\theta = 97.5^\circ$ . For the inflow region, the value of  $e\Phi_{\parallel}$  can be inferred from the 'shoulder' in  $f(\varepsilon, \theta)$  observed in the parallel direction<sup>14,20,26</sup>.

Meanwhile, the strong energization of the flat-top distributions in the reconnection exhaust, up to more than ten times the initial ion temperature ( $\sim 1$  keV), is not well understood and has so far not been reproduced in kinetic simulations of reconnection. The observations of the flat-top distributions call for a highly efficient mechanism for converting magnetic energy into electron kinetic energy during the reconnection process. Below we present results from a large-scale kinetic simulation that reproduces the electron energization in the exhaust by electrons accelerated directly in parallel electric fields as characterized by  $e\Phi_{\parallel}$ . The heating mechanism is also consistent with the flat energization spectra observed for the superthermal electrons<sup>12</sup>.

<sup>1</sup>Massachusetts Institute of Technology, Plasma Science and Fusion Center, Cambridge, Massachusetts 02139, USA, <sup>2</sup>Los Alamos National Laboratory, Los Alamos, New Mexico 87545, USA. \*e-mail: jgedal@psfc.mit.edu.

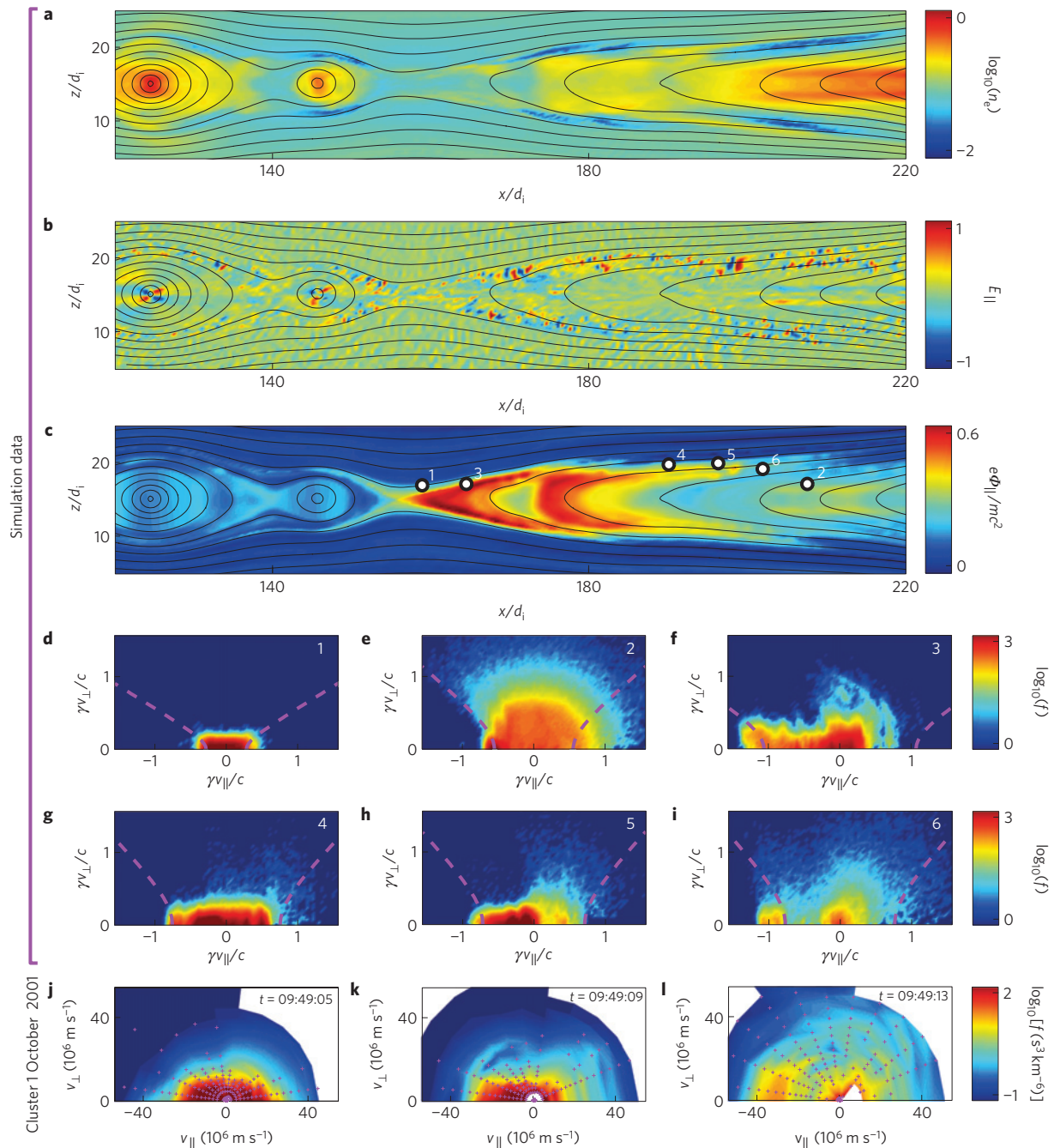


**Figure 2 | Kinetic simulation results and spacecraft data demonstrating electron energization by parallel electric fields. a–c.** Contours of constant  $n_e$ ,  $E_{\parallel}$  and  $e\Phi_{\parallel}$ , respectively. **d–i.** Electron distributions for the points marked in **c**. The magenta lines indicate the trapped passing boundaries. **j–l.** Electron distributions recorded by spacecraft Cluster 1 in a separator crossing. The magenta dots indicate the locations of measurements in velocity space. The simulated distributions in **g–i** qualitatively match these experimental distributions.

The two-dimensional simulation was carried out on the Kraken petascale supercomputer, using the kinetic particle-in-cell code VPIC (ref. 13), which solves the relativistic Vlasov–Maxwell system of equations. The case described here is initialized with a Harris current sheet and further details regarding the set-up are given in the Methods section.

The present simulation differs from previous two-dimensional simulations in two important aspects. First, it uses a low value of the normalized upstream electron pressure,  $\beta_{e\infty} = 2\mu_0 p_{eb}/B_0^2 = 0.0028$ , lower by a factor of 18 when compared with most previous investigations. Here  $p_{eb}$  and  $B_0$  are the upstream values of the electron pressure and magnetic field, and  $\mu_0$  is the vacuum

permeability. The reduced value of  $\beta_{e\infty}$  is applied to be in better agreement with the dataset from the Cluster mission discussed above<sup>14</sup> and because new theoretical results have shown that  $e\Phi_{\parallel}/T_{eb}$  becomes large at small values of  $\beta_{e\infty}$  (ref. 15). Here  $T_{eb}$  is the upstream electron temperature (Methods). Second, most previous simulation domains have spanned an area of the order of  $20d_i \times 20d_i$  or less, where  $d_i$  is the ion inertial length. For the present simulation the domain is much larger ( $320d_i \times 30d_i$ ), such that the boundary conditions do not limit the size of the regions where electrons are energized over the time considered.

Figure 2a–c shows the profiles of the electron density,  $n_e$ , the parallel electric field,  $E_{\parallel}$ , and  $\Phi_{\parallel}$ . Along the separators (the

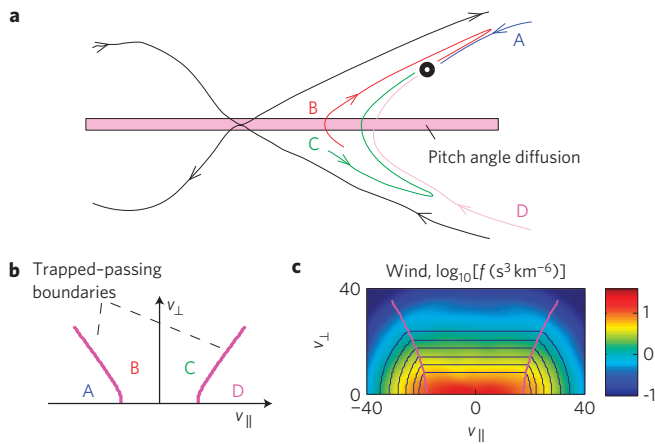


**Figure 3 | Classification of electron trajectories near a magnetic separator.** **a**, Representative electron trajectories reaching a point in the exhaust region. Trajectories A and D are ‘passing’ while trajectories B and C are trapped. Strong pitch-angle diffusion occurs at the midplane where the magnetic field is weak and the field lines bend strongly. **b**, Regions in the  $(v_{\parallel}, v_{\perp})$  plane corresponding to the four classes of electron trajectories. The magenta lines represent the trapped–passing boundaries. **c**, Colour contours of an inflow electron distribution function recorded by the Wind spacecraft at 08:00:22 UT on 1 April 1999 (ref. 2). The black contour lines are obtained from the theoretical model of refs 20,26.

magnetic-field lines connected to the  $x$  line), cavities are observed where  $n_e$  is reduced by almost an order of magnitude from the upstream value. Within these cavities, strong alternating parallel electric fields are observed, which is the signature of so-called electron holes. In previous simulations such structures have been observed in the vicinity of the electron-diffusion region in guide-field reconnection along two of the four separators<sup>16</sup>. In contrast, here the cavities are observed along all four separators and travel downstream with the exhaust as new sets of cavities form close to the reconnection site. Below we discuss the formation of electron beams inside the cavities (Fig. 2i), which are the likely driver of the electron holes. The magnitude of  $\Phi_{\parallel}$  increases dramatically within the density cavities, corresponding to an average  $E_{\parallel}$  pointing away from the reconnection region, which accelerates electrons towards the region, consistent with observations in magnetopause reconnection<sup>17</sup>. The magnitude of  $\Phi_{\parallel}$  and the spatial extent of  $\Phi_{\parallel}$  are decisively enhanced when compared with previous results. The value of  $e\Phi_{\parallel} \sim 0.7m_e c^2$  is about an order of magnitude larger than previous results, and the region where  $e\Phi_{\parallel}$  is large fills the entire exhaust, reaching about  $60d_i$  downstream to the right of the reconnection region. In the left exhaust, secondary magnetic islands are observed, which suppresses the values of  $e\Phi_{\parallel}$  by about a factor of two. Scans in the size of the simulation domain and the value of  $\beta_{\infty}$  show that it is the low value of  $\beta_{\infty}$  that is responsible for the large value of  $e\Phi_{\parallel}$  observed. As described in the methods section, the normalized potential,  $e\Phi_{\parallel}/T_{eb}$ , should be used when comparing with spacecraft data. We find that the simulation value of  $e\Phi_{\parallel}/T_{eb} \sim 90$  is in good agreement with the values inferred from the shoulder energy of the exhaust flat-top distributions recorded by the Cluster mission (Fig. 1c). While not shown here, the reconnection region is characterized by electron-pressure anisotropy,  $p_{\parallel} \gg p_{\perp}$ , which drives extended electron jets as previously studied<sup>15</sup>.

In Fig. 2c six points are selected for which the respective electron distributions as a function of the parallel and the perpendicular velocities,  $(v_{\parallel}, v_{\perp})$ , are shown in Fig. 2d–i. In agreement with the Cluster observations discussed above, the distribution in Fig. 2d demonstrates the heating along the parallel direction characteristic

for electrons in the inflow region. Observations of parallel heating in the inflow are common and accurately accounted for in an analytic theory involving the electron response to  $\Phi_{\parallel}$  (Fig. 3c). Also consistent with the Cluster observations, in the distribution in Fig. 2e for point 2 located within the exhaust, we observe a flat-top distribution where  $f(\varepsilon)$  is near constant for  $\varepsilon < 0.4m_e c^2$ . The dashed magenta lines represent the trapped–passing boundaries, which are controlled by the local values of  $\Phi_{\parallel}$  and  $B$ . These boundaries are important for the structure of  $f(v_{\parallel}, v_{\perp})$  and will be discussed below.

Near point 3 in the exhaust close to the  $x$  line and separator the largest values of  $\Phi_{\parallel}$  are observed. The resulting distribution (Fig. 2c) shows electrons heated up to  $|\gamma v_{\parallel}| \sim 1.4c$  in the direction of incoming electrons. Meanwhile, the distributions in Fig. 2g–i of points 4, 5 and 6 facilitate a direct comparison with distributions in Fig. 2j–l measured by Cluster 1 during a separator crossing. In both simulation and spacecraft data we observe a gradual change from distributions heated in only the parallel and anti-parallel directions into hot isotropic distributions with a clear beam feature superimposed. In both the simulation and the experimental data, the beam is travelling towards the reconnection region, a feature that is commonly observed in separator crossings<sup>18,19</sup>.

To understand how the various distributions are formed, it is important to consider the underlying electron dynamics. Because of their low mass, electrons rapidly move along magnetic-field lines while slowly convecting with the field lines through the reconnection region. In Fig. 3a we consider different classes of electron trajectories reaching the point marked in the exhaust region. The trajectories marked by A and D we denote as passing, as these pass through the reconnection region along field lines without any reflections. Meanwhile, the trajectories marked B and C we denote as trapped, because they bounce back and forth along field lines as the magnetic field lines convect into the reconnection region. Especially at low energies, the trapped trajectories can be more complicated than indicated, including trapping in local structures of the parallel electric field. However, these details do not significantly influence the overall form of the electron distributions, which are largely determined by how the trapped and passing trajectories partition the  $(v_{\parallel}, v_{\perp})$  plane as shown in Fig. 3b. The boundary between regions A and B and the boundary between regions C and D we denote as the trapped–passing boundaries, and these are readily characterized in terms of the local values of  $\Phi_{\parallel}$  and  $B$  (ref. 20).

To account for the flat-top distribution in Fig. 2e it is important to note that not only will  $\Phi_{\parallel}$  accelerate ‘new’ electrons into the region, it will also help confine the hot electrons that entered the region at earlier times. For the flat-top distribution, only electrons in region D of the  $(v_{\parallel}, v_{\perp})$  plane will escape the reconnection region. Meanwhile, the intense beam of incoming electrons in region ‘A’ will be well confined as it reaches the midplane and the pitch angle scatters mainly into regions B and C because the characteristic Larmor radius is larger than the curvature radius of the magnetic field<sup>21</sup>. Thus, the electrons escaping with high parallel energies  $\varepsilon_{\infty} > e\Phi_{\parallel}$  in region D are being replaced by nearly fixed-energy electrons ( $\varepsilon = e\Phi_{\parallel}$ ). In principle, this will lead to a distribution peaked at  $\varepsilon = e\Phi_{\parallel}$ , but such non-monotonic features in  $f(\varepsilon)$  are highly unstable, leading to instabilities including the observed electron hole formation<sup>22</sup>. This causes electrons to scatter to lower energies such that  $f(\varepsilon)$  is ‘flat’ for  $\varepsilon < e\Phi_{\parallel}$ . In agreement with our interpretation, for the distribution in Fig. 2e the trapped–passing boundary between regions A and B is clearly visible and agrees fully with that calculated using the observed values of  $B$  and  $\Phi_{\parallel}$  (the magenta line). In addition, we note the presence of the incoming beam in region A setting the shoulder energy of the flat-top distribution.

In the present simulation, we find that  $en\Phi_{\parallel} \approx B_0^2/(2\mu_0)$ , such that the pressure of the flat-top distributions largely balances the

upstream magnetic-field pressure. Using this condition of pressure balance an upper limit is obtained,  $e\Phi_{\parallel}/T_{\text{eb}} \approx (n_0/n)(T_{\text{e0}} + T_{\text{i0}})/T_{\text{eb}}$ . Because the density of the exhaust,  $n$ , is similar to that of the lobe plasma,  $n_b$ , the magnitude of  $e\Phi_{\parallel}/T_{\text{eb}}$  becomes substantial. We also note that, whereas the magnetic energy dissipation mainly occurs in the density cavities remote from the  $x$  line, the most energetic distributions are observed closer to the  $x$  line where  $e\Phi_{\parallel}$  is maximal.

In the simulation, the area of large values of  $e\Phi_{\parallel}$  fills the entire exhaust and its spatial extent is clearly not limited to the kinetic length scales  $d_e$  or  $d_i$ . This suggests that energization by  $e\Phi_{\parallel}$  may also be applicable to solar flares, where electrons are rapidly energized at the onset of reconnection strongly enough to balance the external magnetic-field pressure (as is the case here) in regions that are six orders of magnitude larger than  $d_i$  (ref. 23). We note that our new energization mechanism could also be important to flare models invoking incremental energization at multiple reconnection sites between magnetic islands and flux ropes. In such large systems,  $E_{\parallel}$  may also be important for accelerating ions. However, more work is still required to determine if the spatial extent of  $e\Phi_{\parallel}$  increases proportionally to the system size and if the large values of  $e\Phi_{\parallel}$  persist in more complicated geometries including a strong guide magnetic field.

## Methods

The two-dimensional kinetic simulation<sup>13</sup> is initialized with a Harris<sup>24</sup> neutral sheet with magnetic field profile  $B_x = B_0 \tanh(z/d_i)$ . To better mimic the magnetotail, open boundary conditions<sup>25</sup> are employed in the  $x$  and  $z$  directions. Following previous two-dimensional studies<sup>25</sup>, a weak 3% magnetic perturbation is included to initiate reconnection within the central region. The initial particle distribution included counter-drifting Maxwellian ion and electron populations localized to support the Harris current layer and along with a separate uniform background resulting in a total density profile  $n(z) = n_0 \text{sech}^2(z/d_i) + n_b$ . Here  $n_0$  is the central Harris density,  $n_b$  is a uniform background density and  $n_b/n_0 = 0.05$  for this simulation. The ion-to-electron temperature ratio of the Harris population is  $T_{i0}/T_{e0} = 5$ , whereas the temperatures,  $T_{ib}$  and  $T_{eb}$ , for the uniform background populations have the same ratio, but are a factor of three colder for both species. Lengths are normalized by the ion  $d_i = c/\omega_{pi}$  and electron  $d_e = c/\omega_{pe}$  inertial scales, where  $\omega_{ps} = (4\pi e^2 n_0/m_s)^{1/2}$  for each species  $s = i, e$ . The domain size is  $L_x \times L_z = 320d_i \times 30d_i$ , corresponding to  $40,960 \times 3,840$  cells. The simulation used 600 particles per cell for each species for a total of 188 billion particles. Other parameters are  $m_i/m_e = 400$  and  $\omega_{pe}/\Omega_{ce} = 2$ , where  $\Omega_{ce} = eB_0/(m_e c)$  and the time step was  $\Delta t \omega_{pe} = 0.1$ . The simulation results shown in Fig. 2 correspond to time  $t\Omega_{ci} = 61$ . The unit of energy in the simulation is  $m_e c^2$ , but as a standard measure to save computational resources the initial temperatures of the background plasma,  $T_{ib} \sim m_e c^2/29$  and  $T_{eb} \sim m_e c^2/144$ , are much larger than the corresponding values in the Earth magnetotail (about 1 keV and 200 eV, respectively). Therefore, when comparing with the magnetotail the relevant quantities must be renormalized in terms of the applied values of  $T_{ib}$  and  $T_{eb}$ . Fully three-dimensional simulations have been carried out for the antiparallel scenario studied here and two-dimensional simulations with  $m_i/m_e = 1,836$  have also been completed. Although those simulations applied smaller simulation domains they show that the heating mechanism described here is robust also in three dimensions and at full mass ratio between the electrons and ions.

Received 28 July 2011; accepted 27 January 2012; published online 26 February 2012

## References

- Dungey, J. Conditions for the occurrence of electrical discharges in astrophysical systems. *Phil. Mag.* **44**, 725–738 (1953).
- Oieroset, M., Lin, R. & Phan, T. Evidence for electron acceleration up to 300 keV in the magnetic reconnection diffusion region of Earth's magnetotail. *Phys. Rev. Lett.* **89**, 195001 (2002).
- Lin, R. & Hudson, H. 10–100 keV electron acceleration and emission from solar flares. *Sol. Phys.* **17**, 412–435 (1971).
- Lin, R., Krucker, S., Hurford, G. J., Smith, D. M. & Hudson, H. S. Rhesi observations of particle acceleration and energy release in an intense solar gamma-ray line flare. *Astrophys. J.* **595**, L69–L76 (2003).
- Holman, G. Energetic electrons in solar flares as viewed in X-rays. *Adv. Space Res.* **35**, 1669–1674 (2005).
- Abdo, A. A. *et al.* & The Fermi Collaboration. Gamma-ray flares from the crab nebula. *Science* **331**, 739–742 (2011).
- Birn, J. *et al.* Geospace environmental modeling (GEM) magnetic reconnection challenge. *J. Geophys. Res.* **106**, 3715–3719 (2001).
- Wygant, J. R. *et al.* Cluster observations of an intense normal component of the electric field at a thin reconnecting current sheet in the tail and its role in the shock-like acceleration of the ion fluid into the separatrix region. *Geophys. Res.* **110**, A09206 (2005).
- Chen, L. J. *et al.* Observation of energetic electrons within magnetic islands. *Nature Phys.* **4**, 19–23 (2008).
- Asano, Y. *et al.* Electron flat-top distributions around the magnetic reconnection region. *J. Geophys. Res.* **113**, A01207 (2008).
- Egedal, J., Daughton, W., Drake, J. F., Katz, N. & Le, A. Formation of a localized acceleration potential during magnetic reconnection with a guide field. *Phys. Plasmas* **16**, 050701 (2009).
- Egedal, J. *et al.* Cause of super-thermal electron heating during magnetotail reconnection. *Geophys. Res. Lett.* **37**, L10102 (2010).
- Bowers, K. J., Albright, B. J., Yin, L., Bergen, B. & Kwan, T. J. T. Ultrahigh performance three-dimensional electromagnetic relativistic kinetic plasma simulation. *Phys. Plasmas* **15**, 055703 (2008).
- Egedal, J. *et al.* Cluster observations of bidirectional beams caused by electron trapping during antiparallel reconnection. *J. Geophys. Res.* **115**, A03214 (2010).
- Le, A. *et al.* Magnitude of the Hall fields during magnetic reconnection. *Geophys. Res. Lett.* **37**, L03106 (2010).
- Drake, J. F. *et al.* Formation of electron holes and particle energization during magnetic reconnection. *Science* **299**, 873–877 (2003).
- Mozer, F. S. & Pritchett, P. L. Spatial, temporal, and amplitude characteristics of parallel electric fields associated with subsolar magnetic field reconnection. *J. Geophys. Res.* **115**, A04220 (2010).
- Nagai, T. *et al.* Evidence of magnetic reconnection in the magnetotail. *J. Geophys. Res.* **106**, 25929–25949 (2001).
- Manapat, M., Oieroset, M., Phan, T., Lin, R. & Fujimoto, M. Field-aligned electrons at the lobe/plasma sheet boundary in the mid-to-distant magnetotail and their association with reconnection. *Geophys. Res. Lett.* **33**, L05101 (2006).
- Egedal, J. *et al.* Evidence and theory for trapped electrons in guide field magnetotail reconnection. *J. Geophys. Res.* **113**, A12207 (2008).
- Buchner, J. & Zelenyi, L. Regular and chaotic charged-particle motion in magnetotail-like field reversals. *J. Geophys. Res.* **94**, 11821–11842 (1989).
- Omura, Y., Matsumoto, H., Miyake, T. & Kojima, H. Electron beam instabilities as generation mechanism of electrostatic solitary waves in the magnetotail. *J. Geophys. Res.* **101**, 2685–2697 (1996).
- Krucker, S. *et al.* Measurements of the coronal acceleration region of a solar flare. *Astrophys. J.* **714**, 1108–1119 (2010).
- Harris, E. G. On a plasma sheath separating regions of oppositely directed magnetic field. *Nuovo Cimento* **23**, 115–121 (1962).
- Daughton, W., Scudder, J. & Karimabadi, H. Fully kinetic simulations of undriven magnetic reconnection with open boundary conditions. *Phys. Plasmas* **13**, 072101 (2006).
- Egedal, J. *et al.* *In situ* discovery of an electrostatic potential, trapping electrons and mediating fast reconnection in the Earth's magnetotail. *Phys. Rev. Lett.* **94**, 025006 (2005).

## Acknowledgements

We gratefully acknowledge support from NASA (National Aeronautics and Space Administration) through grant NNX10AL11G, and National Science Foundation (NSF) CAREER grant 0844620, both at MIT. Contributions from W.D. were supported by NASA's Heliophysics Theory Program and by the US Department of Energy through the Los Alamos National Laboratory (LANL)/Laboratory Directed Research and Development Program. Initial simulations were carried out using LANL institutional computing resources and the Pleiades computer at NASA, while the final simulation was carried out on Kraken with an allocation of advanced computing resources provided by the National Science Foundation at the National Institute for Computational Sciences (<http://www.nics.tennessee.edu/>). We also thank L.-J. Chen and B. Lefebvre for access to electron data from the Cluster mission.

## Author contributions

J.E. carried out the data analysis and wrote the paper. W.D. carried out the simulation. All of the authors worked on the theoretical interpretation, discussed the results and commented on the paper.

## Additional information

The authors declare no competing financial interests. Reprints and permissions information is available online at [www.nature.com/reprints](http://www.nature.com/reprints). Correspondence and requests for materials should be addressed to J.E.